RSC Advances

ROYAL SOCIETY OF CHEMISTRY

www.rsc.org/advances

Doxycycline conjugated with polyvinylpyrrolidone-encapsulated silver nanoparticles*:* a polymer's malevolent touch against *Escherichia coli*

Heloiza F. O. Silva[1], Kássio M. G. Lima[1], Mateus B. Cardoso[2], Jessica Fernanda Affonso de Oliveira[2], Maria C. N. Melo[3], Celso Sant'Anna[4], Mateus Eugênio[4] and Luiz H. S. Gasparotto[1*]

[1]Group of Biological Chemistry and Chemometrics, Institute of Chemistry, Federal University of Rio Grande do Norte, Natal 59072-970, RN-Brasil.

[2] LNLS – Brazilian Synchrotron Light Laboratory CEP 13083-970, Caixa Postal 6192, Campinas, SP, Brazil

[3]Laboratory of Medical Bacteriology, Center of Biosciences, Federal University of Rio Grande do Norte, Natal 59078-970, RN-Brasil.

[4]Laboratory of Biotechnology – Labio, National Institute of Metrology, Quality and technology – Inmetro, Duque de Caxias 25250-020, RJ-Brazil

Keywords: green synthesis; silver nanoparticles; antibiotic conjugation; antibacterial effect.

**Corresponding author: Dr. Luiz H. S. Gasparotto (lhgasparotto@ufrnet.br) +55 84 33422323*

Doxycycline conjugated with polyvinylpyrrolidone-encapsulated silver nanoparticles: a polymer's malevolent touch against *Escherichia coli*

Abstract

The emergence of multi-resistant pathogens has catapulted research to new strategies to cope with this ever-increasing issue. In this context we combined silver nanoparticles (AgNPs) with doxycycline (DO, an antibiotic from the class of tetracyclines) to evaluate the potentiality of this hybrid as a bactericidal agent against *E. coli*. Polyvinylpyrrolidone (PVP) was used as stabilizer to prevent excessive growth and agglomeration of AgNPs. Interestingly, DO bound directly to PVP and had its concentration increased around the particle as a consequence of that interaction. As a result, the AgNPs/DO conjugates presented enhanced bactericidal properties compared to the individual components. Stabilizing agents are normally unwanted on the surface of nanoparticles because their block potential adsorption surface sites. However, we have shown that PVP played a paramount role in concentrating DO around the particle, which culminated in an increased bactericidal activity towards *E. coli*.

Graphical abstract

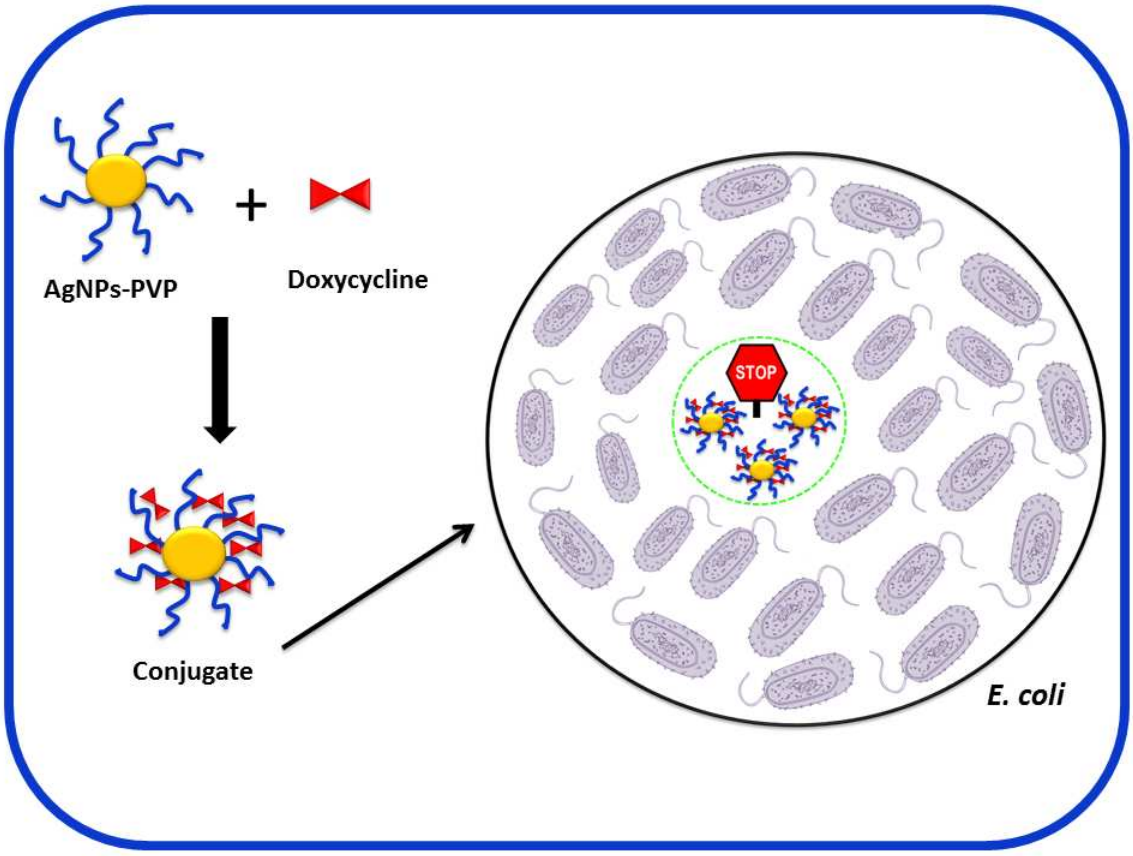

Interaction of silver PVP-capped silver nanoparticles with doxyciline enhances bactericidal properties

1 – Introduction

Silver has long been known to present antimicrobial activity [1-4], but the advent of antibiotics has severely decreased its use for bactericidal purposes. The ability of various microorganisms to adapt to antimicrobial drugs and the improper administration of antibiotics have enabled the emergence of multidrug-resistant pathogens [5, 6], for which the treatment with broad-spectrum antibiotics is less effective, more toxic, and expensive. The latter facts led to the renaissance of the silver-based bactericidal agents, especially in the nanoregime [7-10], which display considerable broad-spectrum antimicrobial activity. An interesting approach is the combination of nanoparticles and antibiotics to yield a more potent antimicrobial agent [11, 12]. Due to their large surface-area-to-volume ratio and biocompatibility, inorganic nanoparticles are considered ideal candidates for carrying large amounts of antibiotics without compromising their activity. Li *et al*. [13] showed that the combination of silver nanoparticles with amoxicillin resulted in greater bactericidal effect on *Escherichia coli* than when the components are administered separately. Rai *et al*. [14] used cefaclor, a second-generation antibiotic, as reducing and capping agents to produce spherical gold nanoparticles. The authors showed nanogold-cefaclor hybrid to have potent antimicrobial activity against both Gram-positive (*Staphylococcus aureus*) and Gram-negative (*Escherichia coli*) bacteria. The conjugation of antibiotics with inorganic nanoparticles might be a strategy against multidrug-resistant bacteria.

In this work we showed that the combination of polyvinylpyrrolidone (PVP)-capped silver nanoparticles (AgNPs) with doxycycline (DO), an antibiotic from the class of the tetracyclines, yields a hybrid agent for the inhibition of *E. coli*. The results showed that PVP had a key role in linking DO to the nanoparticle, thus the system profits from the combination of the intrinsic bactericidal properties of silver with the increased concentration of the DO around the particle. To our knowledge this is the first report on combining DO with a polymer-coated silver nanoparticle. This process might be suitable for coating surgical instruments, implants, and other surfaces that require hygienic conditions.

2 – Experimental section

2.1 – *Chemicals and reagents*

Silver nitrate, polyvinylpyrrolidone (PVP, molecular weight = 10.000), sodium hydroxide, glycerol and DO hyclate (> 98%) were all products of Sigma-Aldrich Chemical Co. *Escherichia coli* strain INCQS 00171 was cultivated in our laboratory.

2.2 – Production and characterization of AgNPs

AgNPs were produced using a previously reported method [15, 16]. Briefly, all glassware was kept overnight in $KMnO_4$ + NaOH solution, rinsed with deionized water, kept for 10 min in H_2O_2 + H_2SO_4 solution (1:1 v/v), again rinsed with deionized water and dried prior to use. The following stock solutions were prepared: 50 mmol L^{-1} $AgNO_3$, 166 g l^{-1} PVP, and a solution containing 1.0 mol L^{-1} NaOH + 1.0 mol L^{-1} glycerol. Known volumes of the PVP and $AgNO_3$ solutions were dissolved in water to yield a 5-mL solution. In a separate beaker, a determined volume of the NaOH + glycerol solution was mixed in water to generate a 5-mL solution. Afterwards, the glycerol-NaOH solution was added to the $AgNO_3$-PVP one to yield the final concentrations displayed in Table 1, where can be seen the coded and real values for the 2^2 full factorial design conceived with the help of the software MODDE® 4.0 from Umetrics, Umeå, Sweden). The AgNPs colloidal solutions had then their pH adjusted to 7 by addition of diluted HCl.

UV-vis absorption spectra of the AgNPs were acquired with an Evolution 60S UV-visible spectrophotometer (Thermo Scientific). Dynamic light scattering (DLS) and fluorescence spectroscopy were carried out with a ZetaPlus instrument and a Perkin Elmer LS45 fluorometer, respectively. Small-angle x-ray scattering (SAXS) was conducted on the D1B beamline at the Brazilian Synchrotron Light Laboratory (LNLS). For this liquid samples (water as solvent) were injected into an in-vacuum cell with parallel mica windows at a sample-to-

detector distance of 1500 mm. The monochromatized X-ray beam had a wavelength of 1.488 nm and the detector was a Pilatus 300k. FTIR in the ATR mode was performed with a Bruker Vertex 70 spectrophotometer.

2.3 – Conjugation of DO with AgNPs

Conjugation of AgNPs with DO was achieved by simple incubation. Different volumes of a 10 mmol L^{-1} doxycxcline stock solution were added to the AgNPs colloidal solutions to produce distinct concentrations of the antibiotic. All the above-mentioned techniques were used to characterize the AgNPs-antibiotic complex.

2.4 – Bacteriological experiments

E. coli was cultured in Müller-Hinton agar medium on a Petri dish at 37 ^{o}C for 24 h. Then bacteria colonies were transferred into a 0.9 % saline solution to yield a suspension with a turbidity of 0.5 MaCFarland that is equivalent to 1 x 10^{8} UFC mL^{-1}. The latter suspension was then swabbed onto another Petri dish containing the Müller-Hinton agar medium. Afterwards, with the help of a sterilized stainless-steel cylinder, 6-mm wells were made in the culture medium and filled with 50 μL of the antimicrobial agents (DO, AgNPs, and DO conjugated with AgNPs). The plates were incubated at 37 ^{o}C for 24 h and had their inhibition zones recorded and expressed in the millimeter unit.

3 – Results and discussion

3.1 – Synthesis and characterization of AgNPs

In this work AgNPs were synthesized by reducing Ag^+ with glycerol in alkaline medium at room temperature. The current production of glycerol is sufficient for its main use as raw material in pharmaceutical and cosmetics industries. As glycerol is now also produced as a byproduct of the biodiesel fabrication, the availability of this alcohol surpassed its current demand making it a relatively inexpensive chemical [17]. Due to its biodegradability under aerobic conditions, non-toxicity, and low price, glycerol is a more attractive option for generating nanoparticles when compared to current reducing chemicals such as formamide, sodium borohydride and hydrazine. Based on preliminary UV-vis results from our group, glycerol alone is not capable to act concomitantly as reducing and stabilizing agents, thus the use of a capping agent is imperative to prevent aggregation and precipitation of AgNPs. PVP has been elected for the task due to its intrinsic non-toxicity [18] and capping properties [15, 16, 19]. Table 1 shows the coded levels and real values with their effect on the size of the AgNPs. As the results were acquired with DLS, what is indeed probed is the hydrodynamic diameter of the particles, meaning that the measured size takes into account the adsorbed PVP. In Table 1 shows that large nanoparticles (96.6 nm ± 2.1 nm) are obtained at the lowest PVP and Ag^+ concentrations and a possible agglomeration can not be ruled out either. In contrast, the highest

values of the variables generated smaller nanoparticles with narrower size distribution (22.3 nm ± 0.6). These results are summarized in Fig. 1, in which one can note that both factors, PVP and Ag^+, are relevant to determine the size of the nanoparticles, however the Ag^+ concentration was found to deliver the most pronounced effect on the size of the AgNPs. This is probably due to the autocatalytic nature of the AgNPs formation process [20]. The AgNPs initially pass through a latency period whose length depends on the Ag^+ concentration. At high Ag^+ concentration many nuclei are rapidly formed which, in turn, speed up the reaction since they serve as seeds for $Ag^+ \rightarrow Ag^0$. At low Ag^+ concentration the process is overall slower, thus silver is preferably incorporated in the few formed nuclei, which leads to bigger particles.

The pH was kept at 13 because alkaline media are imperative for the synthesis of silver nanoparticles, as shown previously for silver [15] and gold [21]. Fig. 2A reveals the effect of the PVP concentration on the UV-vis spectra of the AgNPs, with silver concentration kept at 1 mmol L^{-1}. For the PVP concentration of 5.0 g/L [PVP(+)] the spectrum is centered at 400 nm, a value that corresponds to the characteristic surface plasmon resonance (SPR) of PVP-stabilized AgNPs [15] in the same chemical environment. The absence of multiple bands is an indicative of isotropic AgNPs [22], which will be confirmed later by TEM. Additionally, the symmetry of the band suggests low degree of aggregation in the solution [23]. The lowest concentration of PVP [PVP(-)] caused a slight redshift of the maximum wavelength that is now at 407 nm, suggesting an overall particle size increase [24]. Fig. 2B depicts the impact of

Ag^+ concentration of the shape of UV-vis spectra of AgNPs with PVP kept at its highest value. At low Ag^+ concentration [Ag^+(-)] the spectrum is redshifted compared to that from high Ag^+ concentration, hence corroborating the results from DLS that show a particle size increase.

All the AgNPs samples were analyzed with TEM and the results are shown in Fig. 2C. The size distribution of the Ag(+)PVP(+) sample clearly presents a bimodal feature, with the first and second populations having average sizes of 2.9 nm ± 1.0 nm and 15.1 nm ± 5.1 nm. A bimodal size distribution stems from the dissolution of small particles and redeposition of the dissolved species onto the surface of larger particles, hence spawning two particle populations. It is important to point out that the over 70 % of the nanoparticles are comprised in the population centered at 2.9 nm, as seen in the respective histogram. Once the average particle size increases the bimodal feature tends to disappear, as in the case of the Ag(+)PVP(-) sample whose average size distribution is 4.0 nm (± 1.8 nm). The size distribution broadened slightly as a consequence of the low PVP amount, a result corroborated by UV-vis. The size of AgNPs substantially increased when the Ag^+ concentration was set at its lowest value. The Ag(-)PVP(+) and Ag(-)PVP(-) presented average sizes of 24 nm ± 8.0 nm and 18.0 ± 22 nm, respectively. In the case of the latter (at the lowest PVP amount), the standard deviation was substantially larger than that of the former due to the low PVP concentration that led to a poor capping capacity. This is consistent with results in Fig. 1, which demonstrated that the lowest concentrations of both Ag^+ and PVP generated larger nanoparticles with broader

size distributions. It is interesting to notice that DLS significantly overestimates the size of the nanoparticles since it measures the hydrodynamic radius, which takes into account the layer of adsorbed PVP.

3.2 – Conjugation of DO with AgNPs

The next step comprises the conjugation of the AgNPs with DO, which in principle can be monitored via quenching of the AgNPs fluorescence signal. Fig. 3A shows fluorescence emission spectra of AgNPs at distinct concentrations of DO. One readily sees that the lowest concentration of DO (16 μmol L^{-1}) is sufficient to cause some fluorescence quenching and that at the concentration of 144 μmol L^{-1} the fluorescence signal is practically suppressed. Fig 3B presents the fluorescence intensity before the addition of DO (F_0) over the fluorescence intensity (F) after the addition of DO. The plot deviates from the classic Stern-Volmer behavior, which suggests a non-linear DO-AgNPs interaction [25]. A somewhat linear behavior is observed only at low DO concentrations. Non-linear Stern-Volmer plots are often found for macromolecules [26] and nanoparticles [27] and are normally attributed to static quenching [28]. However, in our case, we may have to consider the possibility that the DO is simply within the “sphere of action” of the fluorophore, a situation in which the quencher (DO) is close enough to the fluorophore at the moment of excitation and instantly quenches the excited state [29]. This hypothesis is supported by the existence of a capping polymer that might prevent DO to directly bind to the AgNPs. In order to shed

light into this matter fluorescence lifetime experiments were conducted for AgNPs in the absence and presence of DO, with results shown in the inset of Fig. 3B. Analysis of the plots gave essentially the same lifetimes, being 6.90 ns and 7.25 ns for AgNPs and AgNPs mixed with DO, respectively, suggesting that the DO is not adsorbed directly onto the AgNPs. Nevertheless DO is being accumulated near the AgNPs as depicted by Fig. 3B. A plausible explanation would be that the capping polymer, the PVP, is interacting with DO causing its accumulation at the nanoparticle's surface.

Fig. 4 presents FTIR spectra in ATR mode of DO, DO mixed with AgNPs, and DO mixed only with PVP. The molecular structure of DO (scheme 1) is also provided for clarification. As the most characteristic region of the DO spectrum comprises the range of 1200 – 1800 cm^{-1}, only this region has been analyzed in detail. The bands have been assigned according to the studies of Gu and Karthikeyan [30] and Lacher *et al.* [31]. DO (black line) had its bands assigned as follows: frequencies at 1677 cm^{-1} and 1537 cm^{-1} are related to the carbonyl and amino groups of the amide, respectively, in ring A; bands at 1613 cm^{-1} and 1581 cm^{-1} correspond to the carbonyl groups in rings A and C, respectively; the band at 1458 cm^{-1} is related to the C=C skeleton vibration. The oxygens on C1 and C3 may be equivalent since there was only one frequency at 1615 cm^{-1} [32]. The spectrum of DO mixed with PVP-capped AgNPs (Fig. 4A, blue line) clearly shows band changes of amide carbonyl and amino groups in ring A. Upon mixing DO with PVP-capped AgNPs the amide C=O of DO shifted from 1677 cm^{-1} to 1670 cm^{-1} and the $–NH_2$ went from 1536 cm^{-1} to 1542 cm^{-1}. These results

suggest that the DO complexation with PVP could take place through the amide C=O in ring A. These shifts have also been observed in the spectrum of DO mixed with PVP alone, as depicted in Fig. 4B, which corroborates the idea that DO is interacting mainly with PVP.

Another point worth mentioning in Fig. 4A is the increased band signal upon addition of AgNPs into DO solution. As ATR is a technique that probes the interfacial region between the solution and the ATR crystal, more intense signals mean higher concentration of the in-question species at the interface. Due to the ease to draw a baseline, the bands at 1582 cm^{-1} were chosen to be integrated and compared with that of pure DO, as depicted in Fig. 5. In the latter graphic it is clearly observed that the addition of PVP-capped AgNPs into the DO solution provoked an increase of band intensity, which is justified by an increased concentration of DO around the particle promoted by the polymer. This interpretation is in consonance with the fluorescence results of Fig. 3B, in which the fluorescence quenching is brought in by high concentrations of DO due to PVP-DO interaction. Interestingly, PVP itself is not able to promote a local concentration increase (Fig. 5), which suggests that the structure and concentration of PVP around the nanoparticle may also play a role in encapsulating DO. AgNPs produced with the lowest and highest PVP concentration promoted 6 % and 20 % increase of DO concentration around the particles, respectively.

The UV-vis spectra of DO and DO mixed with PVP-capped AgNPs in Fig. 6 further prove that these species interact with each other. UV-vis spectrum of

DO (red curve) has a maximum at 346 nm that is shifted to 363 nm upon mixing with AgNPs (blue curve). This implies that the tricarbonylamide group in ring A is involved in the complexation with PVP, which is corroborated by the ATR experiments presented in Fig. 4. Further SAXS measurements (Fig. 7) revealed that DO has practically no effect on the size of the AgNPs as well as in their distribution, an important result that can rule out size effects in the bacteriological tests.

3.3 – Antimicrobial tests

The well-diffusion method was adopted to access the antimicrobial potentiality of the AgNPs as well as the AgNPs-DO. As shown in Fig. 8 *E. coli* had its growth inhibited by the conjugates, which is denoted by the round lighter-shaded area around the wells. In those photographs the inhibition zone in the center of the Petri dishes was due to a DO solution used as a control to check on the bacteria susceptibility to antibiotics. It is important to stress that the DO concentration of 30 μg/mL in the control was the same used in all the conjugates.

Fig. 9 summarizes the antibacterial results from the conjugates and some important features can be promptly realized from it. The components (glycerol and PVP) used to synthesize the nanoparticles were found not to present any antibacterial effect (results not shown). AgNPs produced with the highest concentration of Ag^+ successfully prevented bacteria growth, meaning that conjugation-free particles are also efficient for this purpose. At the same silver

loading, the Ag(+)PVP(+) nanoparticles delivered somewhat larger inhibition zones than the Ag(+)PVP(-) probably because the latter are slightly bigger than the former. It has been discussed in the literature that small silver nanoparticles are more active than bigger ones due to their larger surface-area-to-volume ratio of the former, which leads to a larger contact area between the nanoparticles and bacteria [33]. Another mechanism is the uptake of free silver ions that are released by the AgNPs followed by disruption of ATP production and increase of DNA mutation [34]. Naturally, smaller AgNPs release more silver ions than larger ones, therefore preventing bacteria growth more efficiently. Upon conjugation of AgNPs with DO it was observed that the inhibition zones of the conjugates are larger than those of the respective AgNPs alone. It was also to expect that the conjugates delivered inhibition zones larger than those calculated by summing the inhibition zones of the components alone (DO + AgNPs). However, inspection of the results in Fig. 9 shows that it was not the case for the Ag(+)PVP(+) and Ag(+)PVP(-) conjugates. It is well known that tetracyclines form strong complexes with aluminum and iron [30], and a possible complexation between silver ions and DO can not be ruled out. This could decrease the diffusion of the new species throughout the agar gel, which would in turn spawn smaller inhibition zones in the experiment period. Chin and Lach [35] showed that the diffusion rate of tetracycline chelates is reduced even if the chelate is water soluble.

The most striking results were the antimicrobial activities of the conjugates from nanoparticles produced with the lowest amount o silver ions. One can see in

Fig. 9 that non-conjugated Ag(-)PVP(+) and Ag(-)PVP(-) did not produce any inhibition zones, probably due to the low concentration of nanoparticles and their large size. On the other hand, inhibition zones even larger than that of DO alone were observed for the conjugates Ag(-)PVP(+)/DO and Ag(-)PVP(-)/DO. This may be explained by the ability of the PVP-capped AgNPs to concentrate DO around them, thus locally generating DO concentration greater than the bulk one. We have already discussed in Fig. 5 that even AgNPs with low amount of PVP are capable of concentrating DO. From this result it is clear the pivotal role played by PVP in bonding with DO. As there is now less silver to be released due to the larger size of AgNPs, DO can diffuse away more freely.

4 – Conclusions

Herein we presented a new approach to combine DO with silver nanoparticles. The stabilizing agents are normally unwanted on the surface of nanoparticles because they block potential adsorption surface sites. However, we have shown that PVP played a paramount role in concentrating DO around the particle, which culminated in an increased bactericidal activity towards *E. coli*.

Acknowledgments

The authors are grateful to CNPq (grant 442087/2014-4) and to Prof. Frank H. Quina for the time-resolved fluorescence measurements.

Refrences

(1) Berger, T. J.; Spadaro, J. A.; Chapin, S. E.; Becker, R. O., Electrically generated silver ions: quantitative effects on bacterial and mammalian cells. *Antimicrob. Agents Chemother.* **1976,** 9, 357-358.

(2) Liedberg, H.; Lundeberg, T., Silver alloy coated catheters reduce catheter-associated bacteriuria. *Brit. J. Urol.* **1990,** 65, 379-381.

(3) Jansen, B.; Rinck, M.; Wolbring, P.; Strohmeier, A.; Jahns, T., In vitro evaluation of the antimicrobial efficacy and biocompatibility of a silver-coated central venous catheter. *J. Biomater. Appl.* **1994,** 9, 55-70.

(4) Feng, Q. L.; Wu, J.; Chen, G. Q.; Cui, F. Z.; Kim, T. N.; Kim, J. O., A mechanistic study of the antibacterial effect of silver ions on Escherichia coli and Staphylococcus aureus. *J. Biomed. Mater. Res.* **2000,** 52, 662-668.

(5) Livermore, D. M., Introduction: the challenge of multiresistance. *Int. J. Antimicrob. Agents* **2007,** 29, Supplement 3, S1-S7.

(6) Wright, G. D.; Sutherland, A. D., New strategies for combating multidrug-resistant bacteria. *Trends Mol. Med.* **2007,** 13, 260-267.

(7) Zhang, Y.; Peng, H.; Huang, W.; Zhou, Y.; Yan, D., Facile preparation and characterization of highly antimicrobial colloid Ag or Au nanoparticles. *J. Colloid Interface Sci.* **2008,** 325, 371-376.

(8) Balogh, L.; Swanson, D. R.; Tomalia, D. A.; Hagnauer, G. L.; McManus, A. T., Dendrimer-silver complexes and nanocomposites as antimicrobial agents. *Nano Letters* **2001,** 1, 18-21.

(9) Hernández-Sierra, J. F.; Ruiz, F.; Cruz Pena, D. C.; Martínez-Gutiérrez, F.; Martínez, A. E.; Guillén, A. d. J. P.; Tapia-Pérez, H.; Castañón, G. M., The antimicrobial sensitivity of Streptococcus mutans to nanoparticles of silver, zinc oxide, and gold. *Nanomedicine.* **2008,** 4, 237-240.

(10) Kim, J. S.; Kuk, E.; Yu, K. N.; Kim, J.-H.; Park, S. J.; Lee, H. J.; Kim, S. H.; Park, Y. K.; Park, Y. H.; Hwang, C.-Y.; Kim, Y.-K.; Lee, Y.-S.; Jeong, D. H.; Cho, M.-H., Antimicrobial effects of silver nanoparticles. *Nanomedicine* **2007,** 3, 95-101.

(11) Rosemary, M. J.; MacLaren, I.; Pradeep, T., Investigations of the antibacterial properties of ciprofloxacin@SiO2. *Langmuir* **2006,** 22, 10125-10129.

(12) Jagannathan, R.; Poddar, P.; Prabhune, A., Cephalexin-mediated synthesis of quasi-spherical and anisotropic gold nanoparticles and their in situ capping by the antibiotic. *J. Phys. Chem. C* **2007,** 111, 6933-6938.

(13) Li, P.; Li, J.; Wu, C.; Wu, Q.; Li, J., Synergistic antibacterial effects of β-lactam antibiotic combined with silver nanoparticles. *Nanotechnology* **2005,** 16, 1912.

(14) Rai, A.; Prabhune, A.; Perry, C. C., Antibiotic mediated synthesis of gold nanoparticles with potent antimicrobial activity and their application in antimicrobial coatings. *J. Mater. Chem.* **2010,** 20, 6789-6798.

(15) Garcia, A. C.; Gasparotto, L. H. S.; Gomes, J. F.; Tremiliosi-Filho, G., Straightforward synthesis of carbon-supported Ag nanoparticles and their application for the oxygen reduction reaction. *Electrocatal.* **2012,** 3, 147-152.

(16) Gasparotto, L. H. S.; Garcia, A. C.; Gomes, J. F.; Tremiliosi-Filho, G., Electrocatalytic performance of environmentally friendly synthesized gold nanoparticles towards the borohydride electro-oxidation reaction. *J. Power Sources* **2012,** 218, 73-78.

(17) Gomes, J. F.; de Paula, F. B. C.; Gasparotto, L. H. S.; Tremiliosi-Filho, G., The influence of the Pt crystalline surface orientation on the glycerol electro-oxidation in acidic media. *Electrochim. Acta* **2012,** 76, 88-93.

(18) Nair, B., Final report on the safety assessment of polyvinylpyrrolidone (PVP). *Int. J. Toxicol* **1998,** 17, 95-130.

(19) Pastoriza-Santos, I.; Liz-Marzan, L. M., Formation of PVP-protected metal nanoparticles in DMF. *Langmuir* **2002,** 18, 2888.

(20) Esumi, K.; Hosoya, T.; Suzuki, A.; Torigoe, K., Formation of gold and silver nanoparticles in aqueous solution of sugar-persubstituted poly(amidoamine) dendrimers. *J. Colloid Interface Sci.* **2000,** 226, 346-352.

(21) Ferreira, E. B.; Gomes, J. F.; Tremiliosi-Filho, G.; Gasparotto, L. H. S., One-pot eco-friendly synthesis of gold nanoparticles by glycerol in alkaline medium:

Role of synthesis parameters on the nanoparticles characteristics. *Mater. Res. Bull.* **2014,** 55, 131-136.

(22) Zhang, G.; Jasinski, J.; Howell, J.; Patel, D.; Stephens, D.; Gobin, A., Tunability and stability of gold nanoparticles obtained from chloroauric acid and sodium thiosulfate reaction. *Nanoscale Res. Lett.* **2012,** 7, 337.

(23) Vigneshwaran, N.; Nachane, R. P.; Balasubramanya, R. H.; Varadarajan, P. V., A novel one-pot 'green' synthesis of stable silver nanoparticles using soluble starch. *Carbohydr. Res.* **2006,** 341, 2012-2018.

(24) Daniel, M. C.; Astruc, D., Gold nanoparticles: Assembly, supramolecular chemistry, quantum-size-related properties, and applications toward biology, catalysis, and nanotechnology. *Chem. Rev.* **2004,** 104, 293-346.

(25) Pan, B.; Xing, B.; Liu, W.; Xing, G.; Tao, S., Investigating interactions of phenanthrene with dissolved organic matter: Limitations of Stern-Volmer plot. *Chemosphere* **2007,** 69, 1555-1562.

(26) Lakowicz, J. R.; Weber, G., Quenching of fluorescence by oxygen. Probe for structural fluctuations in macromolecules. *Biochemistry* **1973,** 12, 4161-4170.

(27) Scaiano, J. C.; Laferrière, M.; Galian, R. E.; Maurel, V.; Billone, P., Non-linear effects in the quenching of fluorescent semiconductor nanoparticles by paramagnetic species. *Phys. Status Solidi A* **2006,** 203, 1337-1343.

(28) Keizer, J., Nonlinear fluorescence quenching and the origin of positive curvature in Stern-Volmer plots. *J. Am. Chem. Soc.* **1983,** 105, 1494-1498.

(29) Chris, D. G., Optical halide sensing using fluorescence quenching: theory, simulations and applications - a review. *Meas. Sci. Technol.* **2001,** 12, R53.

(30) Gu, C.; Karthikeyan, K. G., Interaction of tetracycline with aluminum and iron hydrous oxides. *Environ. Sci. Technol.* **2005,** 39, 2660-2667.

(31) Lacher, J. R.; Bitner, J. L.; Park, J. D., The infrared absorption spectra of some antibiotics in antimony trichloride solution. *J. Phys. Chem.* **1955,** 59, 610-614.

(32) Myers, H. M.; Tochon-Danguy, H. J.; Baud, C. A., IR absorption spectrophotometric analysis of the complex formed by tetracycline and synthetic hydroxyapatite. *Calcif. Tissue Int.* **1983,** 35, 745-749.

(33) Rai, M. K.; Deshmukh, S. D.; Ingle, A. P.; Gade, A. K., Silver nanoparticles: the powerful nanoweapon against multidrug-resistant bacteria. *J. Appl. Microbiol.* **2012,** 112, 841-852.

(34) Marambio-Jones, C.; Hoek, E. V., A review of the antibacterial effects of silver nanomaterials and potential implications for human health and the environment. *J. Nanopart. Res.* **2010,** 12, 1531-1551.

(35) Chin, T. F.; Lach, J. L., Drug diffusion and bioavailability: tetracycline metallic chelation. *Am. J. Hosp. Pharm.* **1975,** 32, 625.

Figure captions

Fig. 1 – Effect of Ag^+ and PVP concentrations on the size of AgNPs. Results were acquired with DLS. +1 and -1 represent the highest and lowest concentration values, respectively, of Ag^+ and PVP.

Fig. 2 – Effect of (A) PVP concentration and (B) Ag^+ concentration on UV-vis spectra of the AgNPs. (C) TEM images with the respective size distributions.

Fig. 3 – (A) Fluorescence emission spectra of AgNPs at distinct concentrations of doxycycline, (B) fluorescence intensity before the addition of DO (F_0) over the fluorescence intensity (F) after the addition of different doxycycline concentrations, and (C) fluorescence lifetime of AgNPs in presence and absence of doxycycline.

Fig. 4 – (A) FTIR spectra in ATR mode of 10 mmol L^{-1} doxycycline and 10 mmol L^{-1} doxycycline mixed with AgNPs and (B) 10 mmol L^{-1} doxycycline and 10 mmol L^{-1} doxycycline mixed with 5 g L^{-1} PVP.

Fig. 5 – Effect of the mixing material on the band at 1585 cm^{-1} for DO.

Fig. 6 – UV-vis spectra of DO, AgNPs, and DO mixed with AgNPs.

Fig. 7 – Effect of DO on the size distribution of AgNPs.

Fig. 8 – Inhibition zones for DO conjugated with (A) Ag(+)PVP(+) (left side) and Ag(+)PVP(-) (right side) and (B) Ag(-)PVP(+) (left side) and Ag(-)PVP(-).

Fig. 9 – Bars representation of inhibition zones from well-diffusion experiments carried out with the AgNPs and their respective DO conjugates. NO means “not observed”. Silver loadings: 8.6 μg for Ag(+)PVP(+), Ag(+)PVP(-), and their

conjugates with DO; 0.090 μg for both Ag(-)PVP(+) and its DO conjugate; 0.084 for both Ag(-)PVP(-) and its DO conjugate.

Table 1 - Full factorial experimental design layout

Runs	Coded levels		Real values		Response
	x_1	x_2	Ag^+ (mmol L^{-1})	PVP (g L^{-1})	size / nm
1	+1	-1	1.0	0.50	38.2 ± 0.9
2	+1	+1	1.0	5.0	27.2 ± 0.8
3	+1	+1	1.0	5.0	26.0 ± 0.9
4	-1	+1	0.010	5.0	72.3 ± 2.2
5	+1	-1	1.0	0.50	39.2 ± 0.6
6	-1	+1	0.010	5.0	78.0 ± 5.4
7	-1	-1	0.010	0.50	96.6 ± 2.1
8	-1	-1	0.010	5.0	80.0 ± 3.6
9	+1	-1	1.0	0.50	37.3 ± 2.1
10	+1	+1	1.0	5.0	22.3 ± 0.6
11	+1	+1	1.0	5.0	24.3 ± 0.8
12	-1	+1	0.010	5.0	80.3 ± 7.9
13	+1	-1	1.0	0.50	37.5 ± 2.0
14	-1	+1	0.010	5.0	57.1 ± 3.9
15	-1	-1	0.010	0.50	77.7 ± 5.4
16	-1	-1	0.010	0.50	85.2 ± 2.8

Figure 1

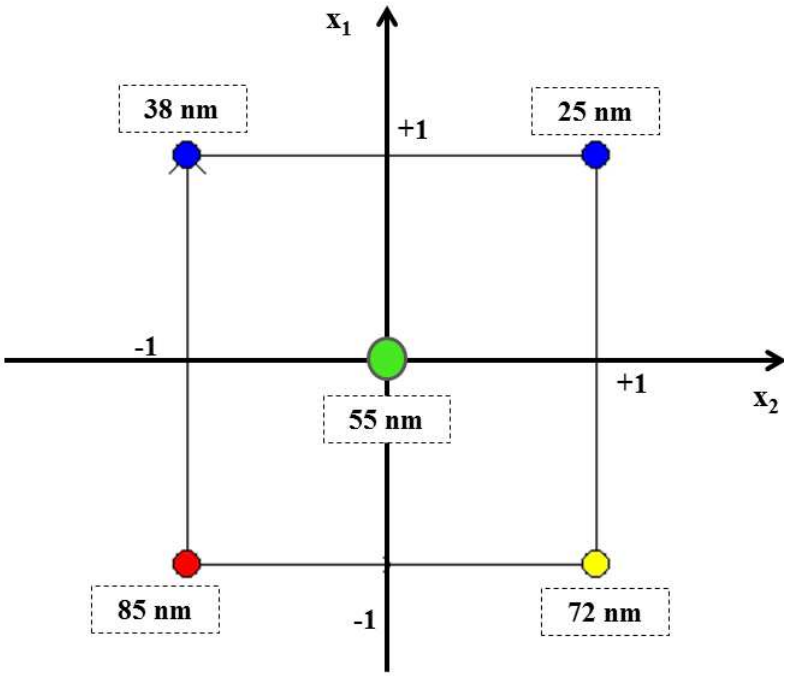

Figure 2

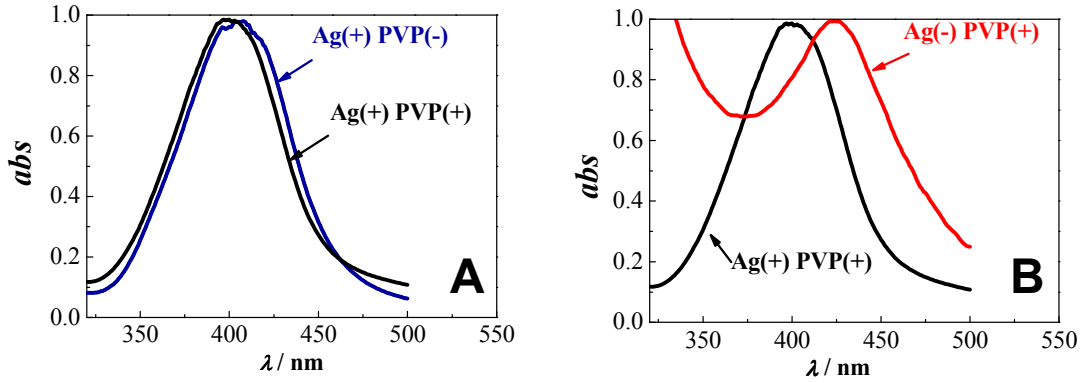

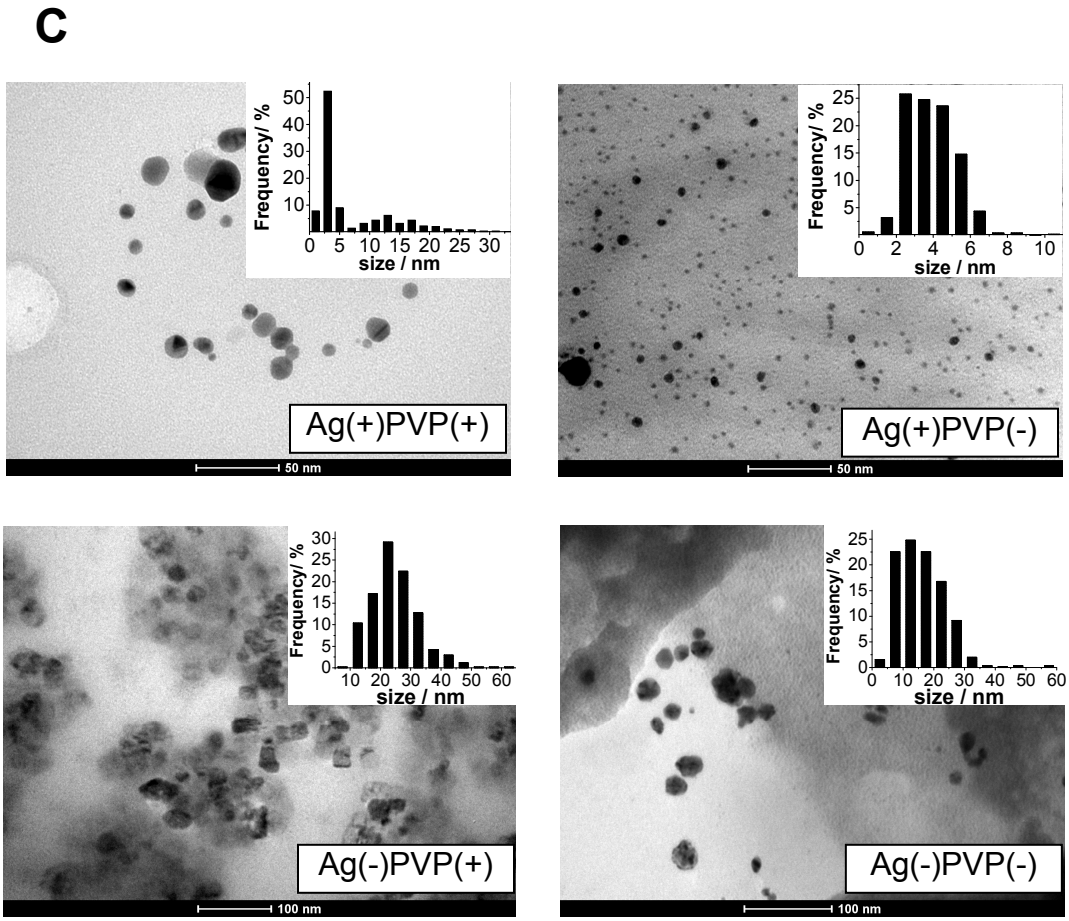

Figure 3

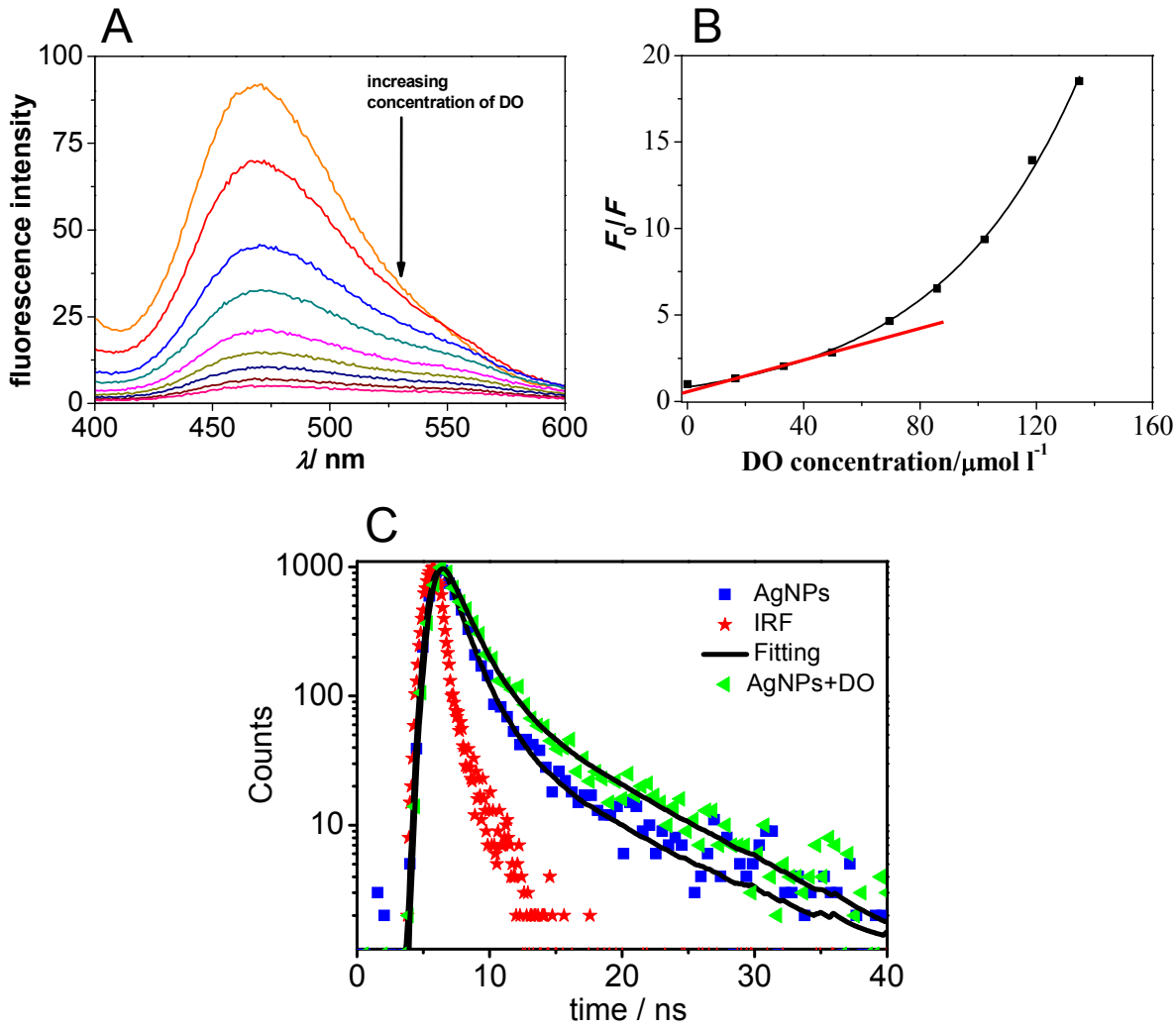

Figure 4

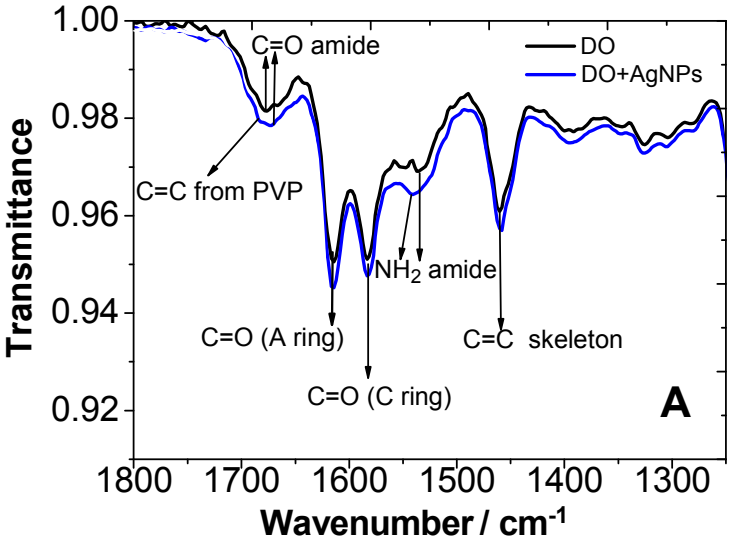

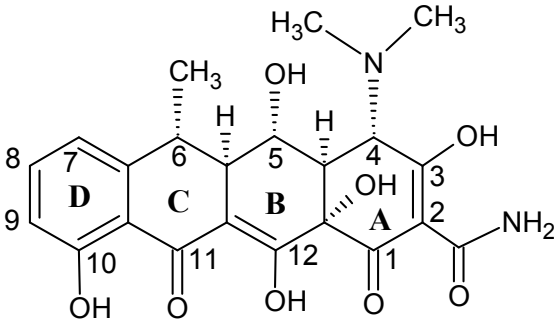

Scheme 1

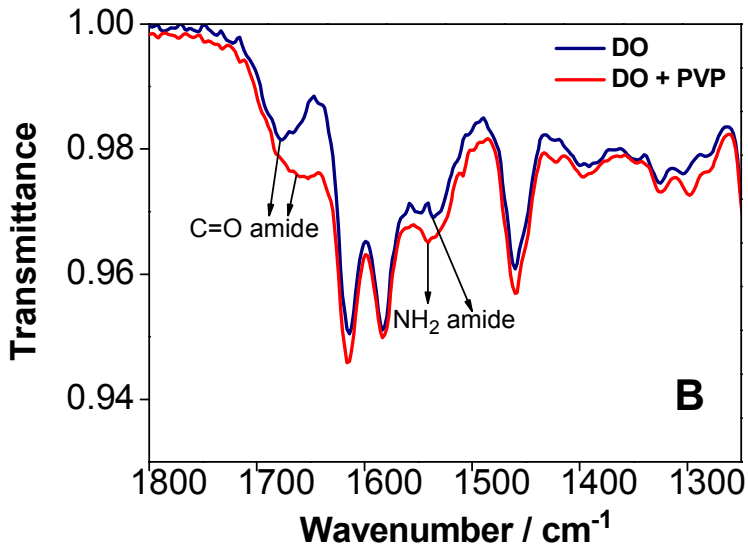

Figure 5

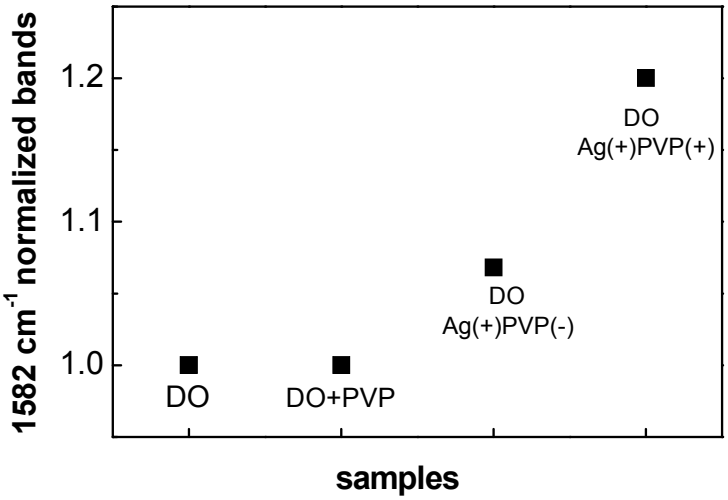

Figure 6

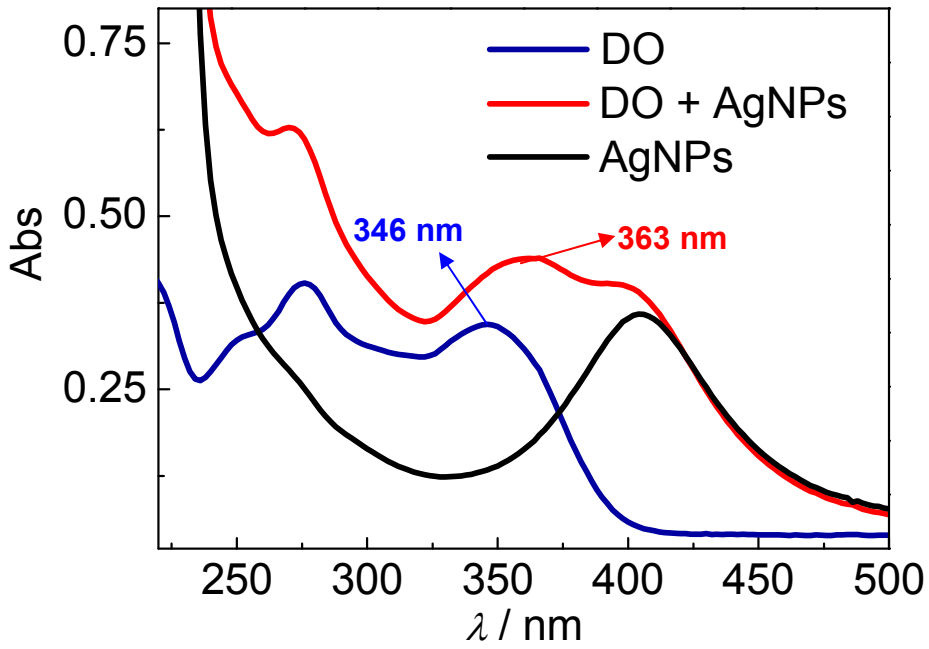

Figure 7

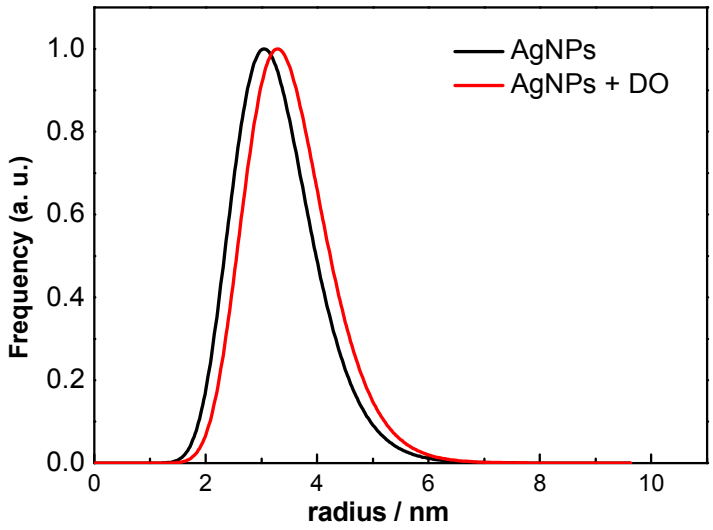

Figure 8

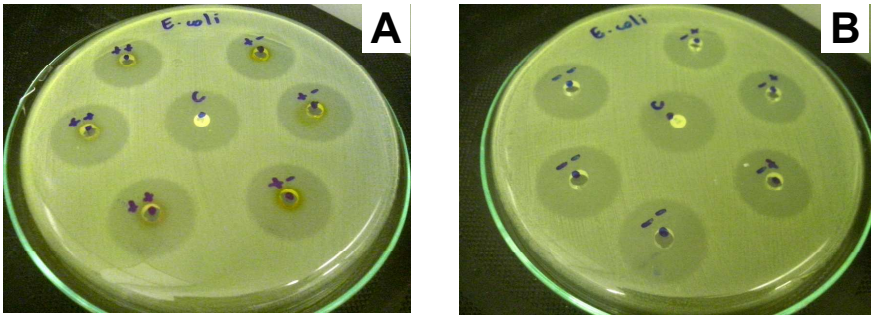

Fig. 9